



Article

Theoretical Study of the Electronic and Magnetic Properties and Phase Stability of the Full Heusler Compound Pd₂CoAl

Liyu Hao ^{1,†}, Jiaxue You ^{1,†}, Rabah Khenata ², Yanfeng Wang ³, Xiaotian Wang ¹  and Tie Yang ^{1,*} 

¹ School of Physical Science and Technology, Southwest University, Chongqing 400715, China

² Laboratoire de Physique Quantique de la Matière et de Modélisation Mathématique, Université de Mascara, Mascara 29000, Algeria

³ College of Sciences, Hebei North University, Zhangjiakou 075000, China

* Correspondence: yangtie@swu.edu.cn

† Authors contributed equally.

Received: 30 July 2019; Accepted: 13 August 2019; Published: 14 August 2019



Abstract: Based on first principles calculation, a systematical investigation has been performed to study the electronic, magnetic, dynamic, and mechanical properties of the full Heusler compound Pd₂CoAl. It is found that the *L*₂₁-type structure is energetically more stable than the *XA*-type due to the lower total energy. The obtained lattice constant in cubic ground state is 6.057 Å, which matches well with previous study. The calculated electronic band structure reveals the metallic nature of Pd₂CoAl and its total magnetic moment of 1.78 μ_B is mainly contributed by Co atom from strong spin splitting effect, as indicated with the distinctive distributions of the density of states in two spin directions. Under uniform strains from −5% to +5%, the variation of total magnetic moment has been obtained and it is still caused by the much larger change from Co atom, compared with Pd and Al atoms. The tetragonal structure has further been analyzed and we found that there is possible martensitic phase transformation because the total energy can be further reduced when the cubic structure is varied into the tetragonal one. The large energy difference of 0.165 eV between the tetragonal and cubic phases is found at the *c/a* ratio of 1.30. The total density of states has been compared between the cubic and tetragonal phases for Pd₂CoAl and results show tetragonal phase transformation could reduce the states at the Fermi energy level in both directions. In addition, the dynamic and mechanical stabilities have also been evaluated for Pd₂CoAl in both cubic and tetragonal structures and results confirm that the tetragonal phase shows good stability against the cubic phase, which further verifies that the tetragonal phase transformation is highly expected. In the end, the strong elastic anisotropy in the tetragonal structure has been clearly shown with the calculated directional dependence of the Young's modulus and shear modulus.

Keywords: first principles calculation; Heusler compounds; electronic band structure; phase transformation

1. Introduction

The family of Heusler alloys has attracted much scientific attention and research interest during recent years, and their various and special functionalities have been extensively studied and explored in many different areas. The ferromagnetism was firstly observed in Heusler compounds with no ferromagnetic elements and, afterwards, many more new properties have been found, such as half metallicity [1–10], spin gapless semiconductivity [11–17], thermoelectricity [18–23], superconductivity [24–26], and topological insulativity [27,28]. Also, these properties can be easily

tuned by simple element substitution within the periodic table. Therefore, ongoing investigations to enhance their performance or even search for new property are still very intense in the scientific community from both theoretical calculation and experimental synthesis. Most of the current applications for Heusler compound are related with the magnetic effect just in different forms, including mainly spintronics and magnetoelectronics.

Normally, Heusler compounds have highly ordered cubic crystal structures with different atomic ordering configurations. However, several recent studies have found many Heusler materials have tetragonal structure as the ground state, e.g., Felser et al. [29] found that $\text{Mn}_{3-x}\text{Fe}_x\text{Ga}$ and $\text{Mn}_{3-x}\text{Co}_x\text{Ga}$ have tetragonal structure over the whole range of compositions from experiment results, and then Faleev et al. [30,31] performed an extensive investigation on the origin of the tetragonal ground state for 286 Heusler compounds by theoretical calculation, which shows 62% have tetragonal structure. More recently, Han et al. [32,33] and Wu et al. [34] studied the phase competition between cubic and tetragonal structures in a series of conventional Heusler compounds Pd_2YZ ($Y = \text{Co, Fe, Mn}$; $Z = \text{B, Al, Ga, In, Tl, Si, Ge, Sn, Pb, P, As, Sb}$) and all-d-metal Heusler compounds $\text{X}_{2-x}\text{Mn}_{1+x}\text{V}$ ($X = \text{Pd, Ni, Pt, Ag, Au, Ir, Co}$; $x = 1, 0$) and Zn_2MMn ($M = \text{Ru, Rh, Pd, Os, Ir}$) and found that many of them also exhibit tetragonal phases, especially the most of Pd_2Co -based Heusler alloys. Compared with the cubic structures, the tetragonal ones have several special properties, like large perpendicular magnetic anisotropy [35–37] and ferromagnetic shape memory behavior [38–43], which are very important for the development of spin-transfer torque magnetic random-access memory, ferromagnetic shape memory alloys and other spintronic applications [29,44–46].

In this work, a detailed study on the full Heusler compound Pd_2CoAl has been carried out with first principles calculation. The electronic and magnetic properties have been calculated based on both cubic and tetragonal structures. Except the general total energy evaluation, the phase stability was further examined by means of both dynamic and mechanical manners and results show that the tetragonal structure has good stability against the cubic counterpart, which further confirms the possible tetragonal phase transformation could be highly expected in this material. Moreover, the elastic anisotropy in the tetragonal structure is revealed with the directional dependence of Young's modulus and shear modulus. This study investigates the phase stability from several different perspectives and thus can give valuable information for the tetragonal state in the palladium-based full Heusler materials or even inspire other similar investigations.

2. Computational Methods and Details

The electronic, magnetic, and mechanical properties of the full Heusler compound Pd_2CoAl have been investigated with the first principles calculations by applying the pseudopotential plane wave methods based on density functional theory [47], as implemented with the CASTEP codes [48]. The Perdew–Burke–Ernzerhof (PBE) 96 in the frame of the generalized gradient approximation (GGA) [49] was selected to describe the electronic exchange correlation energy. The ultrasoft pseudopotential [50] was used to treat the interactions between the valence electrons and the atomic core. The configurations of the valence electrons for Pd, Co, and Al are $4d^{10}$, $3d^7 4s^2$, and $3s^2 3p^1$, respectively. After an initial convergence test, a plane wave cutoff energy of 500 eV has been used together with a k mesh of $12 \times 12 \times 12$ Monkhorst–Pack grid for the Brillouin zone sampling. For the self-consistent field iteration convergence, the difference of the total energy was set to smaller than 1×10^{-6} eV/atom. For the phonon property, the finite displacement method within the density functional perturbation theory [51] has been used.

3. Results and Discussions

3.1. Crystal Structure and Equilibrium Lattice

The Heusler alloys generally have two variants of stoichiometric compositions: the half-Heusler compound with generic formula of XYZ [52–57] and the full Heusler compound X_2YZ [5,58,59],

where X and Y are from transition metal elements and Z from main group elements. In both half and full Heusler alloys, they normally crystalize in a cubic structure yet with different configurations [60]: non-centrosymmetric cubic structure $C1_b$ for half-Heusler; two different types for full Heusler: the Cu_2MnAl structure with space group $Fm\bar{3}m$, also known as $L2_1$ -type, and the Hg_2CuTi structure with space ground $F\bar{4}3m$, also known as “inverse structure” or XA -type. For the currently studied full Heusler compound Pd_2CoAl , the two structural types have been taken into consideration and they are shown in Figure 1. It can be seen that the full Heusler Pd_2CoAl has the general FCC-like symmetry with four interpenetrating sublattices defined by Wyckoff coordinates: $A(0,0,0)$, $B(0.25,0.25,0.25)$, $C(0.5,0.5,0.5)$, and $D(0.75,0.75,0.75)$. In $L2_1$ -type structure, the two Pd atoms occupy the A and C sites, which are symmetrically identical, and the Co and Al atoms enter into the B and D sites, respectively; see Figure 1a. In XA -type structure, the two Pd atoms occupy the A and B sites with different surrounding environments, and the Co and Al atoms enter into the C and D sites; see Figure 1b.

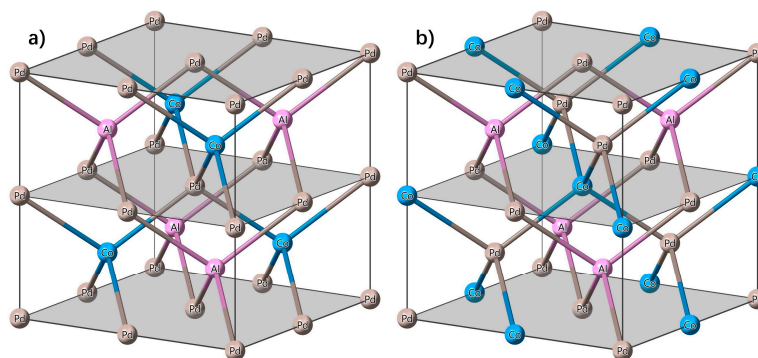


Figure 1. Schematic illustrations of the atomic configurations for the full Heusler compound Pd_2CoAl in (a) $L2_1$ -type and (b) XA -type structures.

In order to determine the ground state structural configuration and also obtain the equilibrium lattice constant, we have calculated the total energy of Pd_2CoAl with different structures under different lattice constants. It should be noted that only the magnetic state is considered, as in the literature [34], since there is Co atom present. The obtained result is reported in Figure 2. It is found that the calculated total energy of Pd_2CoAl in $L2_1$ -type structure is always smaller than in XA -type structure throughout the whole lattice variation range, which means the $L2_1$ -type structure is more energetically preferable and should be the ground state. This observation is in a good agreement with the general site preference rule found in other palladium-based Heusler compounds [32,34], i.e., since the Pd atom has more valence electrons than the Co atom, it is more electronegative and prefers the A and C sites. Thus, the $L2_1$ -type structure is formed for Pd_2CoAl . After the crystal structural configuration of Pd_2CoAl has been determined, we further calculated its equilibrium lattice by polynomial fitting and minimization searching of the total energy and the derived equilibrium lattice is 6.057 Å, see Table 1, which coincides very well with previous study [30,34].

Table 1. The calculated equilibrium lattice constant, total and atom-resolved magnetic moment.

Compound	Lattice (Å)	Magnetic Moment (μ_B)					
		M_{Total} (μ_B)	$M_{\text{Pd(A)}}$	$M_{\text{Pd(B)}}$	M_{Co}	M_{Al}	
Pd_2CoAl	Current	6.057	1.78	−0.06	−0.06	1.95	−0.05
	Ref [34]	6.06	1.79	0.03	0.03	1.75	−0.03

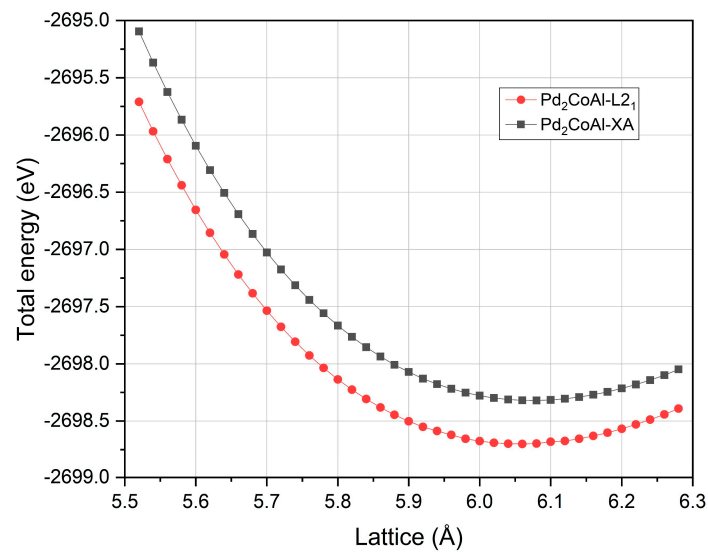


Figure 2. The calculated total energies of the full Heusler compound Pd_2CoAl with different crystal structures under different lattice constants.

3.2. Electronic and Magnetic Properties

With the obtained equilibrium lattice constant, we can then investigate the corresponding electronic and magnetic properties of the full Heusler compound Pd_2CoAl . Firstly, the spin-polarized electronic band structure has been calculated and it is shown in Figure 3. The Fermi energy is shifted to the zero energy level. It can be immediately observed that there are energy bands crossing the Fermi energy level in both spin directions, meaning that this Heusler compound behaves like metallic material at ground state.

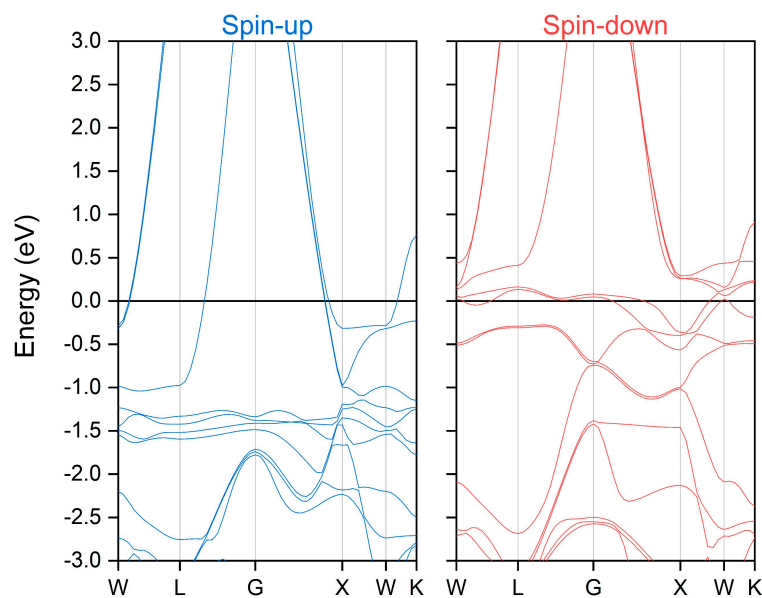


Figure 3. The calculated spin-polarized electronic band structures for the full Heusler compound Pd_2CoAl in L_{21} -type cubic structure at the equilibrium lattice constant.

In order to further elucidate the origin of the magnetism and also access the correlation states between different atoms in Pd_2CoAl , the total and partial densities of states have been also computed and the result is shown in Figure 4. We can find that the main group element Al has negligible contribution and the total density of states is mainly contributed from the d states of the transition metal elements Pd and Co: a roughly symmetric distribution of states between the two spin directions

around -5 to -2 eV from Pd and a strongly asymmetric distribution between the two spin directions around -2 to 1 eV from Co. In particular for the states near the Fermi energy level, they play a very important role in the determination of the electronic and magnetic properties for Heusler compounds. From the total density of states, there is a strong spin splitting effect in the two spin directions with a high peak below the Fermi level in the spin-up direction and a high peak just at the Fermi level in the spin-down direction. A closer look at the partial density of states reveals that this strong spin splitting is caused by the d - d hybridization between the Pd and Co atoms and the strong exchange splitting of the Co atom. The calculated magnetic moments are shown in Table 1, and it is found the total magnetic moment of Pd₂CoAl is about $1.78 \mu_B$ per formula unit and it is mainly from the Co atom. These results for the magnetic moments are consistent with the above analysis from electronic densities.

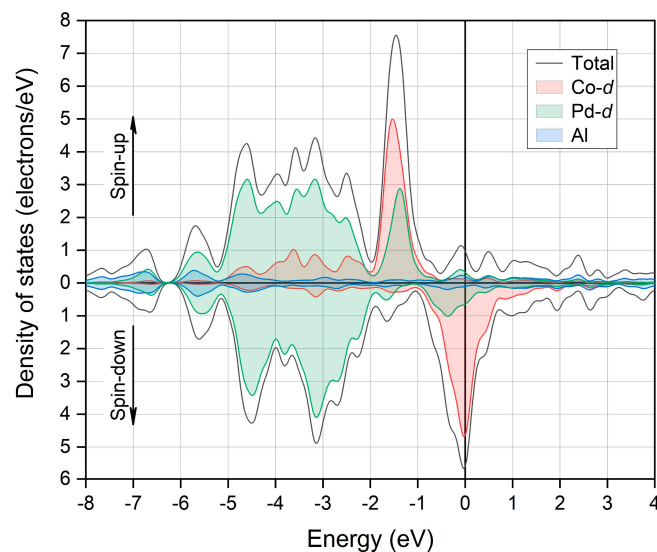


Figure 4. The calculated total and partial densities of states for the full Heusler compound Pd₂CoAl in L₂₁-type cubic structure at the equilibrium lattice constant.

Furthermore, the electronic and magnetic properties of Pd₂CoAl compound under uniform strains have been evaluated with lattice variation from -5% to $+5\%$ with respect to the equilibrium condition. The cubic L₂₁-type structure for Pd₂CoAl under different uniform strains is always maintained. The calculated band structures always exhibit overlaps with the Fermi energy level in both spin directions, indicating the metallic nature of Pd₂CoAl is preserved under uniform strain at the studied range. The total and atom-resolved magnetic moments under uniform strains are displayed in Figure 5. It is found that the magnetic moment of Co atom has quite large variation while the moments of the Pd and Al atoms stay almost constant with strain applied. Note the different scale in different parts of the vertical axis. The total magnetic moment follows the trend of Co atom, which indicates that the strong exchange splitting remains under the studied whole uniform strain. With strain variation from 0% to $-/+5\%$ side, the lattice decreases/increases and the distance between every atom also decreases/increases. Thus, the interaction of the valence electrons from different atoms is decreased with lattice increase and they become more localized, which results in the partial regain of the spin moments from Co atom. It is worth mentioning that the magnetic moments of two Pd atoms are identical and overlap with each other through the whole uniform strain, which is because they have the same surrounding environments in L₂₁-type structure

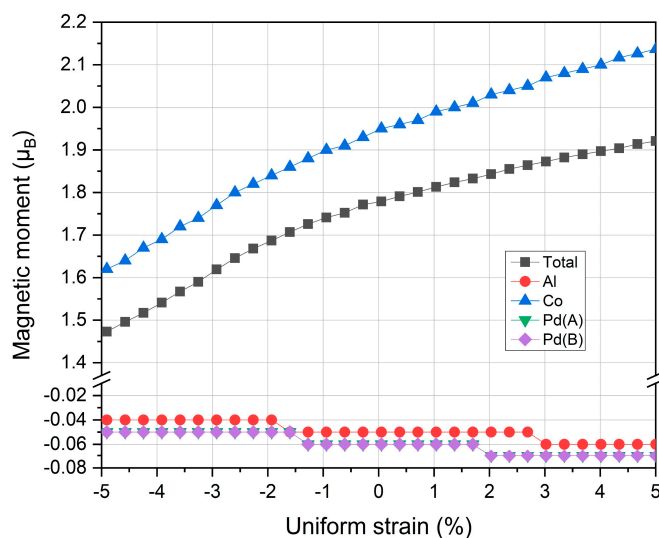


Figure 5. The calculated total and atom-resolved magnetic moments for the full Heusler compound Pd_2CoAl in $L2_1$ -type under different uniform strains. Note the different scale of the two parts in the vertical axis.

3.3. Tetragonal Structure and Phase Stability

In full Heusler compounds with possible phase transformation, the Bain paths have been widely utilized to study the reversible structural transformation between the austenitic and martensitic phases. A recent comprehensive theoretical study [30] of 286 full Heusler alloys from Faleev et al. has found that 62% have tetragonal ground states at zero temperature, including 15 Pd_2 -based full Heusler compounds. It is also well known that the physical properties of solid crystals are strongly related with the corresponding structures. To investigate the phase stability and also its effect in the full Heusler Pd_2CoAl , we further calculate its electronic and magnetic properties under tetragonal structures, which is simply obtained by varying the lattice unproportionally; see Figure 6. Different tetragonal structures are formed by the different c/a ratios, yet the unit cell volume is kept constant, which is the same as the cubic structure. The total energies of the tetragonal phases for Pd_2CoAl under different structure types have been calculated with different c/a ratios and the result is shown in Figure 6. It is seen that there is energy decrease when c/a is deviated from 1 for both structure types, that is, the tetragonal structure could further reduce the system energy and then lead to possible martensitic phase transformation. In comparison, the minimal total energy in the tetragonal XA -type structure is even higher than that in the cubic $L2_1$ -type structure about 0.103 eV, meaning that the $L2_1$ -type structure is energetically stable even under tetragonal structures. The energy minimum in tetragonal $L2_1$ -type structure is found at c/a of 1.30 with energy difference of 0.165 eV relative to the cubic structure; see Figure 6. The energy difference between the cubic austenitic phase and the tetragonal martensitic phase and the c/a ratio at which the tetragonal structure reaches the minimum energy are commonly used to evaluate whether the phase transformation will occur or not in these Heusler compounds. The larger the energy difference is, the more probable the occurrence of the phase transformation is and the more stable the martensitic phase is. Some examples for the energy difference required for stable phase transformation are 0.14 eV and 0.12 eV for Mn_3Ga [61] and Mn_2FeGa [29,31], respectively. The obtained value of 0.165 eV for Pd_2CoAl is even bigger, which implies the stable tetragonal phase could be highly expected. As for the degree of shape memory, the c/a ratio can be used to access this effect and a larger value is preferred.

2.85 states/eV in the martensitic phase. According to the Jahn–Teller effect, this decreasing behavior of the density of states proves that the martensitic phase is more stable than the austenitic phase.

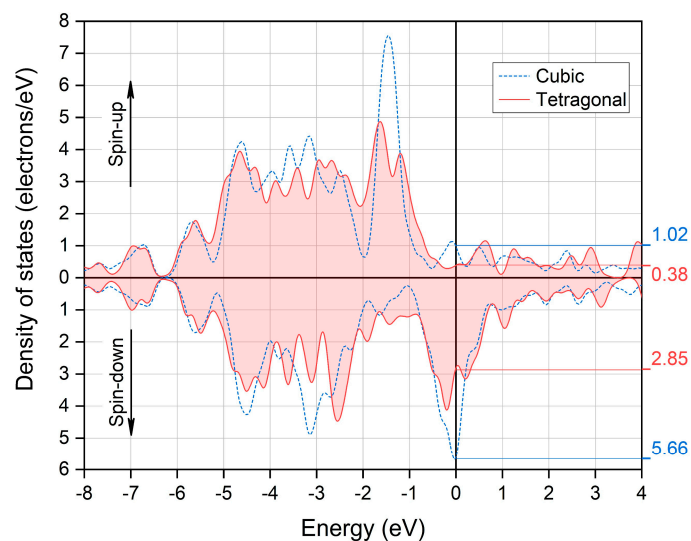


Figure 8. The calculated total densities of states for the full Heusler compound Pd_2CoAl in L_{21} -type cubic and tetragonal structures.

With different tetragonal structures, the total and partial magnetic moments have also been calculated and are displayed in Figure 9. Note the different scale in the two parts of the vertical axis. We can see that the magnetic moment of Co atom always decreases at both sides when c/a ratio is changed from 1, while the moments of Pd atoms decrease at first and then increase, leading to the switch from very weakly antiparallel to weakly parallel. In particular at c/a ratio of 1.30, the magnetic moments of Co and Pd atoms are $1.85 \mu_B$ and $0.07 \mu_B$, respectively. The total magnetic moment is also increased from $1.78 \mu_B$ in the cubic austenitic phase to $1.91 \mu_B$ in the tetragonal martensitic phase.

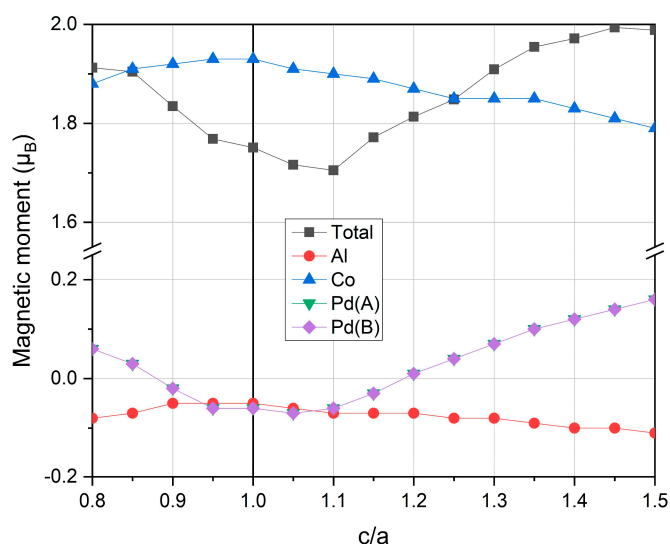


Figure 9. The calculated total and atom-resolved magnetic moments for the full Heusler compound Pd_2CoAl in L_{21} -type structure under different tetragonal strains. Note the different scale of the two parts in the vertical axis.

For the full Heusler compound, the possible martensitic phase transformation can be examined not only with energetic perspective but also by the dynamic and mechanical stability. The phonon dispersion spectra along the high symmetry points in the Brillouin zone for L_{21} -type Pd_2CoAl in both

cubic austenitic and tetragonal martensitic phases have been calculated with the finite displacement method and the results are plotted in Figure 10. It is clearly seen that there is a strong softening behavior present in the cubic structure with a lot of imaginary frequencies, suggesting the structural instability of the austenitic phase. Whereas, the phonon spectrum in the tetragonal structure exhibit no imaginary frequencies and, thus, the system is dynamically stable. This structural instability in the austenitic phase could lead to the martensitic phase transformation.

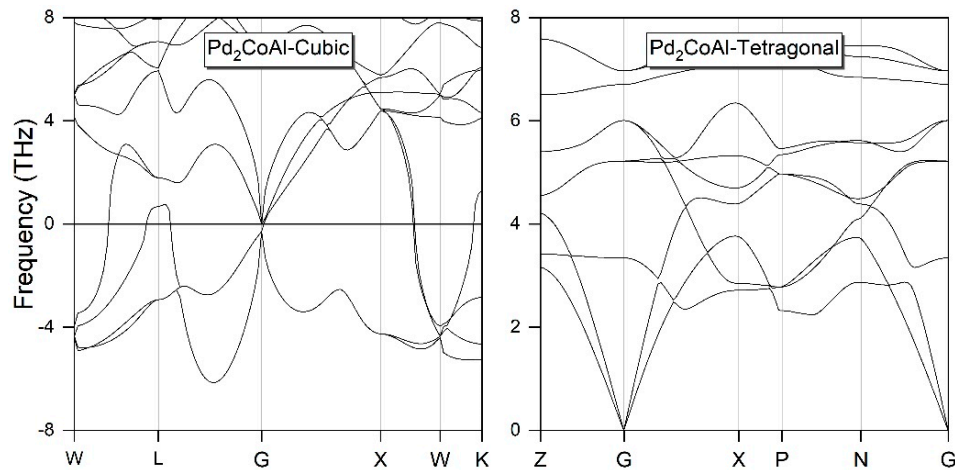


Figure 10. The calculated phonon dispersion spectrum along high symmetry points for the full Heusler compound Pd₂CoAl in L₂₁-type cubic and tetragonal structures.

By employing the stress strain method [62,63], we also computed the various elastic constants for the full Heusler compound Pd₂CoAl in both cubic and tetragonal structures. For a simple cubic structure, there are only three independent elastic constants, namely, C₁₁, C₁₂, and C₁₄. For the tetragonal structure, there are six: C₁₁, C₁₂, C₁₃, C₃₃, C₄₄, and C₆₆. The derived values for all constants are summarized in Table 2. Based on the generalized Born–Huang elastic stability criteria [64], the mechanical stability of Pd₂CoAl in cubic and tetragonal phases should fulfill the following two corresponding conditions:

$$C_{11} + 2C_{12} > 0, C_{11} - C_{12} > 0, C_{44} > 0 \quad (1)$$

$$C_{11} > |C_{12}|, 2C_{13}^2 < C_{33}(C_{11} + C_{12}), C_{44} > 0, C_{66} > 0 \quad (2)$$

From these, we can derive that the cubic phase is not mechanically stable but the tetragonal phase is stable. In combination, the cubic phase Pd₂CoAl is not stable from both the mechanical and dynamic point of view while the tetragonal phase shows good stability, which further elevates the martensitic phase transformation possibility.

Table 2. The calculated various elastic constants (C_{ij}) for the full Heusler compound Pd₂CoAl in both cubic and tetragonal structures.

Compound	Structure	Elastic Constants (GPa)						
		C ₁₁	C ₁₂	C ₁₃	C ₁₄	C ₃₃	C ₄₄	C ₆₆
Pd ₂ CoAl	Cubic	143.2	167.4	-	100.2	-	-	-
	Tetragonal	133.7	38.1	60.3	-	231.2	93.0	86.4

Moreover, with the obtained elastic constants we can further evaluate the elastic anisotropy in the tetragonal L₂₁-type Pd₂CoAl compound. The calculated 3D directional dependence of the Young's modulus and shear modulus with ELATE program [65] are plotted in Figures 11 and 12, respectively. Besides this, the corresponding 2D projections in different planes are also provided together. We can

clearly see that the tetragonal Pd₂CoAl compound has strong elastic anisotropy. The maximum of the Young's modulus and shear modulus are found in the [111] and [001] directions, respectively.

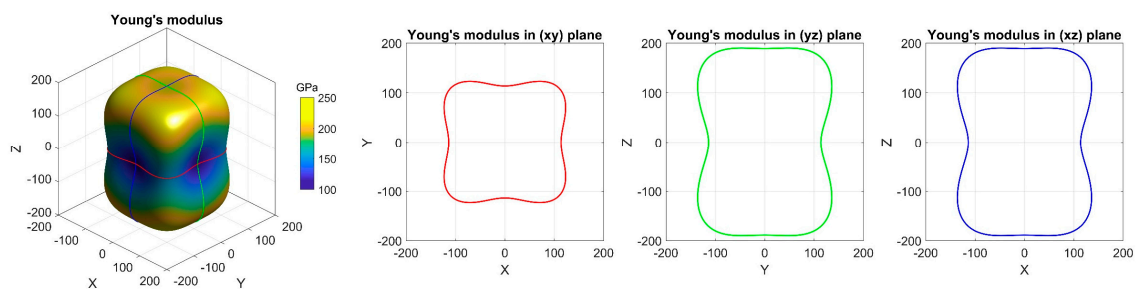


Figure 11. The calculated directional dependent Young's modulus for the full Heusler compound Pd₂CoAl in L₁-type tetragonal structure.

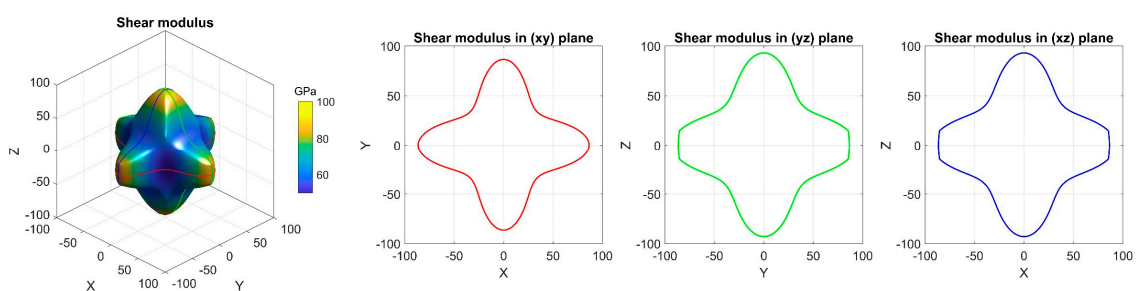


Figure 12. The calculated directional dependent shear modulus for the full Heusler compound Pd₂CoAl in L₁-type tetragonal structure.

4. Conclusions

With first principles calculation, we have systematically investigated the electronic, magnetic, dynamic, and mechanical properties of the full Heusler compound Pd₂CoAl and also examined its phase stability from different perspectives. Results show that the L₂₁-type structure is energetically more preferable than the XA-type because of the lower total energy. The derived equilibrium lattice constant is 6.057 Å and it is in very good agreement with previous study. At ground state in cubic phase, Pd₂CoAl behaves like ferromagnetic metal with total magnetic moment of 1.78 μ_B, which is mainly contributed by the Co atom from strong spin splitting effect of the density of states in two spin directions. Under uniform strains from −5% to +5%, the variation of total magnetic moments has been obtained and it is still caused by the much larger change from the Co atom, compared with Pd and Al atoms. The tetragonal structure has further been considered and it is found the total energy can be reduced when the cubic structure is varied into the tetragonal one, leading to the possible tetragonal martensitic phase transformation. The large energy difference of 0.165 eV between the tetragonal and cubic phases is found at the c/a ratio of 1.30. To evaluate the phase stability, the total density of states has been compared between the cubic and tetragonal phases for Pd₂CoAl, and results show that the tetragonal phase transformation could reduce the states at the Fermi energy level in both directions and thus enhance the phase stability. In addition, the dynamic and mechanical stabilities have also been accessed for Pd₂CoAl in both cubic and tetragonal structures and it is found that the tetragonal phase shows good stability against the cubic phase, which further confirms that the tetragonal phase transformation is highly expected. Lastly, the strong elastic anisotropy has been clearly shown with the 3D representation of the directional dependence of the Young's modulus and shear modulus.

Author Contributions: T.Y. and X.W. conceived the work; L.H. and J.Y. performed the calculations and result analysis and wrote the paper; Y.W. and R.K. provided valuable comments on this work and the manuscript.

Funding: This research was supported by “Fundamental Research Funds for the Central Universities” grant number [XDJK2018C078] and “Doctoral Fund Project of Southwest University” grant number [SWU117037].

Acknowledgments: The authors thank the anonymous reviewers for their constructive suggestions.

Conflicts of Interest: The authors declare no conflict of interest.

References

1. Abada, A.; Amara, K.; Hiadsi, S.; Amrani, B. First principles study of a new half-metallic ferrimagnets Mn₂-based full Heusler compounds: Mn₂ZrSi and Mn₂ZrGe. *J. Magn. Magn. Mater.* **2015**, *388*, 59–67. [[CrossRef](#)]
2. Babiker, S.; Gao, G.; Yao, K. Half-metallicity and magnetism of Heusler alloys Co₂HfZ (Z = Al, Ga, Ge, Sn). *J. Magn. Magn. Mater.* **2017**, *441*, 356–360. [[CrossRef](#)]
3. Bahramian, S.; Ahmadian, F. Half-metallicity and magnetism of quaternary Heusler compounds CoRuTiZ (Z=Si, Ge, and Sn). *J. Magn. Magn. Mater.* **2017**, *424*, 122–129. [[CrossRef](#)]
4. Chen, Y.; Chen, S.; Wang, B.; Wu, B.; Huang, H.; Qin, X.; Li, D.; Yan, W. Half-Metallicity and Magnetism of the Quaternary Heusler Compound TiZrCoIn_{1-x}Gex from the First-Principles Calculations. *Appl. Sci.* **2019**, *9*, 620. [[CrossRef](#)]
5. Galanakis, I.; Dederichs, P.H.; Papanikolaou, N. Slater-Pauling behavior and origin of the half-metallicity of the full-Heusler alloys. *Phys. Rev. B* **2002**, *66*, 174429. [[CrossRef](#)]
6. Galanakis, I.; Mavropoulos, P. Spin-polarization and electronic properties of half-metallic Heusler alloys calculated from first principles. *J. Phys. Condens. Matter* **2007**, *19*, 315213. [[CrossRef](#)] [[PubMed](#)]
7. Ganai, Z.S.; Yousuf, S.; Batoo, K.M.; Khan, M.; Gupta, D.C. Half-metallicity and onsite Hubbard interaction on d-electronic states: A case study of Fe₂NiZ (Z = Al, Ga, Si, Ge) Heusler systems. *Philos. Mag.* **2019**, *99*, 1551–1562. [[CrossRef](#)]
8. Gao, G.Y.; Yao, K.L.; Sasioglu, E.; Sandratskii, L.M.; Liu, Z.L.; Jiang, J.L. Half-metallic ferromagnetism in zinc-blende CaC, SrC, and BaC from first principles. *Phys. Rev. B* **2007**, *75*, 174442. [[CrossRef](#)]
9. Wang, X.T.; Lin, T.T.; Rozale, H.; Dai, X.F.; Liu, G.D. Robust half-metallic properties in inverse Heusler alloys composed of 4d transition metal elements: Zr₂RhZ (Z=Al, Ga, In). *J. Magn. Magn. Mater.* **2016**, *402*, 190–195. [[CrossRef](#)]
10. Yang, T.; Cao, J.T.; Wang, X.T. Structural, Electronic, Magnetic, Mechanic and Thermodynamic Properties of the Inverse Heusler Alloy Ti₂NiIn Under Pressure. *Crystals* **2018**, *8*, 429. [[CrossRef](#)]
11. Bainsla, L.; Mallick, A.I.; Raja, M.M.; Coelho, A.A.; Nigam, A.K.; Johnson, D.D.; Alam, A.; Suresh, K.G. Origin of spin gapless semiconductor behavior in CoFeCrGa: Theory and Experiment. *Phys. Rev. B* **2015**, *92*, 045201. [[CrossRef](#)]
12. Bainsla, L.; Mallick, A.I.; Raja, M.M.; Nigam, A.K.; Varaprasad, B.C.S.; Takahashi, Y.K.; Alam, A.; Suresh, K.G.; Hono, K. Spin gapless semiconducting behavior in equiatomic quaternary CoFeMnSi Heusler alloy. *Phys. Rev. B* **2015**, *91*, 104408. [[CrossRef](#)]
13. Wang, X.L. Proposal for a new class of materials: Spin gapless semiconductors. *Phys. Rev. Lett.* **2008**, *100*, 156404. [[CrossRef](#)]
14. Wang, X.T.; Cheng, Z.X.; Khenata, R.; Rozale, H.; Wang, J.L.; Wang, L.Y.; Guo, R.K.; Liu, G.D. A first-principle investigation of spin-gapless semiconductivity, half-metallicity, and fully-compensated ferrimagnetism property in Mn₂ZnMg inverse Heusler compound. *J. Magn. Magn. Mater.* **2017**, *423*, 285–290. [[CrossRef](#)]
15. Wang, X.T.; Cheng, Z.X.; Wang, J.L.; Wang, X.L.; Liu, G.D. Recent advances in the Heusler based spin-gapless semiconductors. *J. Mater. Chem. C* **2016**, *4*, 7176–7192. [[CrossRef](#)]
16. Wang, X.T.; Li, T.Z.; Cheng, Z.X.; Wang, X.L.; Chen, H. Recent advances in Dirac spin-gapless semiconductors. *Appl. Phys. Rev.* **2018**, *5*, 041103. [[CrossRef](#)]
17. Yang, T.; Hao, L.Y.; Khenata, R.; Wang, X.T. Strain Conditions for the Inverse Heusler Type Fully Compensated Spin-Gapless Semiconductor Ti₂MnAl: A First-Principles Study. *Materials* **2018**, *11*, 2091. [[CrossRef](#)]
18. Chen, X.; Huang, Y.; Yuan, H.; Liu, J.; Chen, H. Theoretical investigation on thermoelectric properties of spin gapless semiconductor Cr₂ZnSi. *Appl. Phys. A* **2018**, *124*, 841. [[CrossRef](#)]
19. Hamad, B. Ab initio investigations of the structural, electronic, and thermoelectric properties of Fe₂NbAl-based alloys. *J. Mater. Sci.* **2016**, *51*, 10887–10896. [[CrossRef](#)]
20. Hasan, R.; Ur, S.C. Thermoelectric and Transport Properties of FeV_{1-x}TixSb Half-Heusler System Synthesized by Controlled Mechanical Alloying Process. *Electron. Mater. Lett.* **2018**, *14*, 725–732. [[CrossRef](#)]

21. Kara, H.; Kahaly, M.U.; Ozdogan, K. Thermoelectric response of quaternary Heusler compound CrVNbZn. *J. Alloy. Compd.* **2018**, *735*, 950–958. [[CrossRef](#)]
22. Lin, T.T.; Gao, Q.; Liu, G.D.; Dai, X.F.; Zhang, X.M.; Zhang, H.B. Dynamical stability, electronic and thermoelectric properties of quaternary ZnFeTiSi Heusler compound. *Curr. Appl. Phys.* **2019**, *19*, 721–727. [[CrossRef](#)]
23. Patel, P.D.; Shinde, S.M.; Gupta, S.D.; Jha, P.K. A promising thermoelectric response of fully compensated ferrimagnetic spin gapless semiconducting Heusler alloy Zr₂MnAl at high temperature: DFT study. *Mater. Res. Express* **2019**, *6*, 076307. [[CrossRef](#)]
24. Shigeta, I.; Kubota, T.; Sakuraba, Y.; Kimura, S.; Awaji, S.; Takanashi, K.; Hiroi, M. Transport properties of epitaxial films for superconductor NbN and half-metallic Heusler alloy Co₂MnSi under high magnetic fields. *Phys. B Condens. Matter* **2018**, *536*, 310–313. [[CrossRef](#)]
25. Nakajima, Y.; Hu, R.; Kirshenbaum, K.; Hughes, A.; Syers, P.; Wang, X.; Wang, K.; Wang, R.; Saha, S.R.; Pratt, D.; et al. Topological RPdBi half-Heusler semimetals: A new family of noncentrosymmetric magnetic superconductors. *Sci Adv.* **2015**, *1*, e1500242. [[CrossRef](#)]
26. Sprungmann, D.; Westerholt, K.; Zabel, H.; Weides, M.; Kohlstedt, H. Evidence for triplet superconductivity in Josephson junctions with barriers of the ferromagnetic Heusler alloy Cu₂MnAl. *Phys. Rev. B* **2010**, *82*, 060505. [[CrossRef](#)]
27. He, M.; Sun, H.; He, Q.L. Topological insulator: Spintronics and quantum computations. *Front. Phys.* **2019**, *14*, 43401. [[CrossRef](#)]
28. Chadov, S.; Qi, X.; Kubler, J.; Fecher, G.H.; Felser, C.; Zhang, S.C. Tunable multifunctional topological insulators in ternary Heusler compounds. *Nat. Mater.* **2010**, *9*, 541–545. [[CrossRef](#)]
29. Felser, C.; Alijani, V.; Winterlik, J.; Chadov, S.; Nayak, A.K. Tetragonal Heusler Compounds for Spintronics. *IEEE Trans. Magn.* **2013**, *49*, 682–685. [[CrossRef](#)]
30. Faleev, S.V.; Ferrante, Y.; Jeong, J.; Samant, M.G.; Jones, B.; Parkin, S.S.P. Origin of the Tetragonal Ground State of Heusler Compounds. *Phys. Rev. Appl.* **2017**, *7*, 034022. [[CrossRef](#)]
31. Faleev, S.V.; Ferrante, Y.; Jeong, J.; Samant, M.G.; Jones, B.; Parkin, S.S.P. Heusler compounds with perpendicular magnetic anisotropy and large tunneling magnetoresistance. *Phys. Rev. Mater.* **2017**, *1*, 024402. [[CrossRef](#)]
32. Han, Y.; Wu, M.; Feng, Y.; Cheng, Z.; Lin, T.; Yang, T.; Khenata, R.; Wang, X. Competition between cubic and tetragonal phases in all-d-metal Heusler alloys, X₂-xMn_{1+x}V (X = Pd, Ni, Pt, Ag, Au, Ir, Co; x = 1, 0): A new potential direction of the Heusler family. *IUCrJ* **2019**, *6*, 465–472. [[CrossRef](#)]
33. Han, Y.L.; Bouhemadou, A.; Khenata, R.; Cheng, Z.X.; Yang, T.; Wang, X.T. Prediction of possible martensitic transformations in all-d-metal Zinc-based Heusler alloys from first-principles. *J. Magn. Magn. Mater.* **2019**, *471*, 49–55. [[CrossRef](#)]
34. Wu, M.; Han, Y.; Bouhemadou, A.; Cheng, Z.; Khenata, R.; Kuang, M.; Wang, X.; Yang, T.; Yuan, H.; Wang, X. Site preference and tetragonal distortion in palladium-rich Heusler alloys. *IUCrJ* **2019**, *6*, 218–225. [[CrossRef](#)]
35. Wu, Y.; Xu, X.G.; Miao, J.; Jiang, Y. Perpendicular Magnetic Anisotropy in Co-Based Full Heusler Alloy Thin Films. *Spin* **2015**, *05*, 1540012. [[CrossRef](#)]
36. Wang, W.H.; Przybylski, M.; Kuch, W.; Chelaru, L.I.; Wang, J.; Lu, Y.F.; Barthel, J.; Meyerheim, H.L.; Kirschner, J. Magnetic properties and spin polarization of Co₂MnSi Heusler alloy thin films epitaxially grown on GaAs(001). *Phys. Rev. B* **2005**, *71*, 144416. [[CrossRef](#)]
37. Huang, B.; Duan, Y.-H.; Hu, W.-C.; Sun, Y.; Chen, S. Structural, anisotropic elastic and thermal properties of MB (M=Ti, Zr and Hf) monoborides. *Ceram. Int.* **2015**, *41*, 6831–6843. [[CrossRef](#)]
38. Fichtner, T.; Wang, C.; Levin, A.A.; Kreiner, G.; Mejia, C.S.; Fabbri, S.; Albertini, F.; Felser, C. Effects of Annealing on the Martensitic Transformation of Ni-Based Ferromagnetic Shape Memory Heusler Alloys and Nanoparticles. *Metals* **2015**, *5*, 484–503. [[CrossRef](#)]
39. Kainuma, R.; Imano, Y.; Ito, W.; Sutou, Y.; Morito, H.; Okamoto, S.; Kitakami, O.; Oikawa, K.; Fujita, A.; Kanomata, T.; et al. Magnetic-field-induced shape recovery by reverse phase transformation. *Nature* **2006**, *439*, 957–960. [[CrossRef](#)]
40. Zhu, W.; Liu, E.K.; Feng, L.; Tang, X.D.; Chen, J.L.; Wu, G.H.; Liu, H.Y.; Meng, F.B.; Luo, H.Z. Magnetic-field-induced transformation in FeMnGa alloys. *Appl. Phys. Lett.* **2009**, *95*, 222512. [[CrossRef](#)]
41. Planes, A.; Mañosa, L.; Acet, M. Magnetocaloric effect and its relation to shape-memory properties in ferromagnetic Heusler alloys. *J. Phys. Condens. Matter* **2009**, *21*, 233201. [[CrossRef](#)]

42. Wei, Z.Y.; Liu, E.K.; Li, Y.; Han, X.L.; Du, Z.W.; Luo, H.Z.; Liu, G.D.; Xi, X.K.; Zhang, H.W.; Wang, W.H.; et al. Magnetostructural martensitic transformations with large volume changes and magneto-strains in all-d-metal Heusler alloys. *Appl. Phys. Lett.* **2016**, *109*, 071904. [[CrossRef](#)]
43. Liu, K.; Ma, S.; Ma, C.; Han, X.; Yu, K.; Yang, S.; Zhang, Z.; Song, Y.; Luo, X.; Chen, C.; et al. Martensitic transformation and giant magneto-functional properties in all-d-metal Ni-Co-Mn-Ti alloy ribbons. *J. Alloy. Compd.* **2019**, *790*, 78–92. [[CrossRef](#)]
44. Zutic, I.; Fabian, J.; Das Sarma, S. Spintronics: Fundamentals and applications. *Rev. Mod. Phys.* **2004**, *76*, 323–410. [[CrossRef](#)]
45. Hirohata, A.; Sagar, J.; Fleet, L.R.; Endo, H. Polycrystalline co-based full-Heusler-alloy films for spintronic devices. *Spin* **2014**, *04*, 1440021. [[CrossRef](#)]
46. Yang, S.A. Dirac and Weyl Materials: Fundamental Aspects and Some Spintronics Applications. *Spin* **2016**, *06*, 1640003. [[CrossRef](#)]
47. Payne, M.C.; Teter, M.P.; Allan, D.C.; Arias, T.A.; Joannopoulos, J.D. Iterative minimization techniques for ab initio total-energy calculations: Molecular dynamics and conjugate gradients. *Rev. Mod. Phys.* **1992**, *64*, 1045–1097. [[CrossRef](#)]
48. Segall, M.D.; Lindan, P.J.D.; Probert, M.J.; Pickard, C.J.; Hasnip, P.J.; Clark, S.J.; Payne, M.C. First-principles simulation: Ideas, illustrations and the CASTEP code. *J. Phys. Condens. Matter* **2002**, *14*, 2717–2744. [[CrossRef](#)]
49. Perdew, J.P.; Burke, K.; Ernzerhof, M. Generalized Gradient Approximation Made Simple. *Phys. Rev. Lett.* **1996**, *77*, 3865–3868. [[CrossRef](#)]
50. Vanderbilt, D. Soft self-consistent pseudopotentials in a generalized eigenvalue formalism. *Phys. Rev. B* **1990**, *41*, 7892–7895. [[CrossRef](#)]
51. Refson, K.; Tulip, P.R.; Clark, S.J. Variational density-functional perturbation theory for dielectrics and lattice dynamics. *Phys. Rev. B* **2006**, *73*, 155114. [[CrossRef](#)]
52. Damewood, L.; Busemeyer, B.; Shaughnessy, M.; Fong, C.Y.; Yang, L.H.; Felser, C. Stabilizing and increasing the magnetic moment of half-metals: The role of Li in half-Heusler LiMnZ (Z=N,P,Si). *Phys. Rev. B* **2015**, *91*, 064409. [[CrossRef](#)]
53. Gofryk, K.; Kaczorowski, D.; Plackowski, T.; Leithe-Jasper, A.; Grin, Y. Magnetic and transport properties of rare-earth-based half-Heusler phases RPdBi: Prospective systems for topological quantum phenomena. *Phys. Rev. B* **2011**, *84*, 035208. [[CrossRef](#)]
54. Karati, A.; Murty, B.S. Synthesis of nanocrystalline half-Heusler TiNiSn by mechanically activated annealing. *Mater. Lett.* **2017**, *205*, 114–117. [[CrossRef](#)]
55. Kroder, J.; Manna, K.; Kriegner, D.; Sukhanov, A.S.; Liu, E.; Borrmann, H.; Hoser, A.; Gooth, J.; Schnelle, W.; Inosov, D.S.; et al. Spin glass behavior in the disordered half-Heusler compound IrMnGa. *Phys. Rev. B* **2019**, *99*, 174410. [[CrossRef](#)]
56. Yin, M.; Nash, P. Standard enthalpies of formation of selected XYZ half-Heusler compounds. *J. Chem. Thermodyn.* **2015**, *91*, 1–7. [[CrossRef](#)]
57. Zilber, T.; Cohen, S.; Fuks, D.; Gelbstein, Y. TiNiSn half-Heusler crystals grown from metallic flux for thermoelectric applications. *J. Alloy. Compd.* **2019**, *781*, 1132–1138. [[CrossRef](#)]
58. Faleev, S.V.; Ferrante, Y.; Jeong, J.; Samant, M.G.; Jones, B.; Parkin, S.S.P. Unified explanation of chemical ordering, the Slater-Pauling rule, and half-metallicity in full Heusler compounds. *Phys. Rev. B* **2017**, *95*, 045140. [[CrossRef](#)]
59. Graf, T.; Casper, F.; Winterlik, J.; Balke, B.; Fecher, G.H.; Felser, C. Crystal Structure of New Heusler Compounds. *Z. Anorg. Allg. Chem.* **2009**, *635*, 976–981. [[CrossRef](#)]
60. Graf, T.; Felser, C.; Parkin, S.S.P. Simple rules for the understanding of Heusler compounds. *Prog. Solid State Chem.* **2011**, *39*, 1–50. [[CrossRef](#)]
61. Liu, Z.H.; Tang, Z.J.; Tan, J.G.; Zhang, Y.J.; Wu, Z.G.; Wang, X.T.; Liu, G.D.; Ma, X.Q. Tailoring structural and magnetic properties of Mn_{3-x}FexGa alloys towards multifunctional applications. *IUCr* **2018**, *5*, 794–800. [[CrossRef](#)]
62. Wang, J.; Li, J.; Yip, S.; Phillpot, S.; Wolf, D. Mechanical instabilities of homogeneous crystals. *Phys. Rev. B* **1995**, *52*, 12627–12635. [[CrossRef](#)]
63. Yip, S.; Li, J.; Tang, M.J.; Wang, J.G. Mechanistic aspects and atomic-level consequences of elastic instabilities in homogeneous crystals. *Mater. Sci. Eng. A Struct. Mater. Prop. Microstruct. Process.* **2001**, *317*, 236–240. [[CrossRef](#)]

64. Mouhat, F.; Coudert, F.X. Necessary and sufficient elastic stability conditions in various crystal systems. *Phys. Rev. B* **2014**, *90*, 224104. [[CrossRef](#)]
65. Gaillac, R.; Pullumbi, P.; Coudert, F.X. ELATE: An open-source online application for analysis and visualization of elastic tensors. *J. Phys. Condens. Matter* **2016**, *28*, 275201. [[CrossRef](#)]



© 2019 by the authors. Licensee MDPI, Basel, Switzerland. This article is an open access article distributed under the terms and conditions of the Creative Commons Attribution (CC BY) license (<http://creativecommons.org/licenses/by/4.0/>).